

A coupled stochastic rainfall-evapotranspiration model for hydrological impact analysis

Minh Tu Pham^{*1}, Hilde Vernieuwe², Bernard De Baets², and Niko E. C. Verhoest¹

¹Laboratory of Hydrology and Water Management, Ghent University, Coupure
links 653, 9000 Ghent, Belgium

²KERMIT, Department of Mathematical Modelling, Statistics and Bioinformatics,
Ghent University, Coupure links 653, 9000 Ghent, Belgium

January 15, 2018

Abstract

A hydrological impact analysis concerns the study of the consequences of certain scenarios on one or more variables or fluxes in the hydrological cycle. In such exercise, discharge is often considered, as floods originating from extremely high discharges often cause damage. Investigating the impact of extreme discharges generally requires long time series of precipitation and evapotranspiration to be used to force a rainfall-runoff model. However, such kind of data may not be available and one should resort to stochastically generated time series, even though the impact of using such data on the overall discharge, and especially on the extreme discharge events, is not well studied. In this paper, stochastically generated rainfall and corresponding evapotranspiration time series, generated by means of vine copulas, are used to force a simple conceptual hydrological model. The results obtained are comparable to the modelled discharge using observed forcing data. Yet, uncertainties in the modelled discharge increase with an increasing number of stochastically generated time series used. Notwithstanding this finding, it can be concluded that using a coupled stochastic rainfall-evapotranspiration model has a large potential for hydrological impact analysis.

1 Introduction

Precipitation is the most important variable in the terrestrial hydrological cycle that determines soil moisture and discharge from a watershed. As such, it also impacts water management where generally the occurrences of extreme events, e.g. storms or droughts, which have very low frequencies, are of concern. Very long time series of precipitation are hence needed. Because this kind of data is not always available, one may consider using a stochastically generated rainfall time series (Boughton and Droop, 2003). Stochastic rainfall models can be used to produce very long time series or to compensate for missing data from finite historical records (Wilks and Wilby, 1999). Several types of rainfall models have been proposed in literature. Onof et al. (2000) grouped all continuous rainfall models into four types: (1) meteorological models; (2) stochastic multi-scale models; (3) statistical models and (4) stochastic process models. Meteorological models are capable to describe the physical processes of all weather variables, including rainfall, by making use of very large and complex sets of equations. Numerical Weather Prediction and General Circulation Models are two common examples of this type of models. Stochastic multi-scale models describe the spatial evolution of the rainfall process regardless of scale factors. In general, these models involve an assumption of temporal invariance of rainfall over a range of scales (Bernardara et al., 2007). Statistical models, which can be used for simulating the precipitation trends, usually treat

^{*}MinhTu.Pham@UGent.be

41 the occurrence and the amount of precipitation separately (Wilks and Wilby, 1999). The rain-
42 fall occurrence is represented by a sequence of dry and wet periods, usually simulated by Markov
43 chains or Alternating Renewal Models. The precipitation amounts can be arbitrarily generated by
44 making use of some popular distributions, e.g. the exponential (Todorovic and Woolhiser, 1975),
45 the Gamma (Stern and Coe, 1984; Viglione et al., 2012) or the mixed exponential distribution
46 (Woolhiser and Roldán, 1982; Wilks, 1998; Mason, 2004). Stochastic process models use simple
47 assumptions of physical processes to simulate the hierarchical structure of the rainfall process.
48 In this approach, only a limited number of parameters is needed (Verhoest et al., 2010). The
49 Bartlett-Lewis (BL) (Rodriguez-Iturbe et al., 1987a) and the Neyman-Scott (Kavvas and Delleur,
50 1981) models are the most commonly used models of this type. In this study, we only focus on
51 the BL models. These models have been applied successfully in different areas, such as Great
52 Britain (Onof and Wheater, 1993; Onof et al., 1994; Cameron et al., 2000), Ireland (Khaliq and
53 Cunnane, 1996), Belgium (Verhoest et al., 1997; Vandenberghe et al., 2010; Vanhaute et al., 2012),
54 the United States of America (Rodriguez-Iturbe et al., 1987b; Velghe et al., 1994), New Zealand
55 (Cowpertwait et al., 2007), Australia (Gyasi-Agyei, 1999; Heneker et al., 2001) and South-Africa
56 (Smithers et al., 2002). The BL models are chosen in this study for three main reasons: (1) they
57 show a good performance in all recent studies; (2) they are capable of generating time series at a
58 sufficient fine time scale (less than 1 hour); (3) their calibration is easy given the limited number
59 of parameters; and (4) they mimic well the stochastic behavior of the historical time series at
60 Uccle (Verhoest et al., 1997; Vanhaute et al., 2012), which is used in this study. The BL model will
61 be employed on a monthly basis such that temporal changes in precipitation characteristics due
62 to the annual cycle can be underpinned. Long-term changes, e.g. due to climate change, however,
63 cannot be accounted for in this model set-up.

64
65 Besides precipitation, the water balance is also highly influenced by the amount of water that
66 is lost due to evapotranspiration. An accurate estimation of evapotranspiration is very essential
67 for hydrological and agricultural designs, irrigation plans and for water distribution management
68 (Droogers and Allen, 2002). The daily reference evapotranspiration is often modelled based on the
69 Penman, Priestley–Taylor or Hargraeves equations; however, one major limitation of these models
70 is that they require extensive input data, such as daily mean temperature, wind speed, relative
71 humidity and solar radiation, which are not always available. Therefore, one may consider to rely
72 on another approach based on stochastically generated time series. More importantly, in order to
73 obtain a correct evaluation of the water balance of a catchment and its discharge, these stochastic
74 evapotranspiration data need to be consistent with the accompanying precipitation time series
75 data (Pham et al., 2016). In this case, we can make use of the copula-based approach introduced
76 in the work of Pham et al. (2016) in which the statistical dependence between evapotranspiration,
77 precipitation and temperature is described by three- and four-dimensional vine copulas.

78
79 Many modelling approaches exist for simulating catchment discharge. The simplest models are
80 the conceptual models in which several (non-)linear reservoirs are put in series and/or parallel.
81 Well-known examples of such conceptual models are: the Hydrologiska Byråns Vattenbalansavdel-
82 ning model (Bergström, 1995), the NedborAfstromnings Model (Nielsen and Hansen, 1973) and
83 the Probability Distributed Model (PDM) (Moore, 2007). Alternatively, physically-based models
84 are based on scientific knowledge of different hydrological processes and their interactions. Gen-
85 erally, these models contain many more parameters than the conceptual ones and require more
86 input data, such as soil type, vegetation-related information, etc. Well-known examples of such
87 models are the Soil and Water Assessment Tool (Arnold et al., 1998), the Système Hydrologique
88 Européen (Abbott et al., 1986) and the Common Land Model (Dai et al., 2003). In this study,
89 we do not intend to seek for the best hydrological model to assess our objective, but we opt for a
90 model that is used in operational water management. More specifically, we will use PDM, as this
91 model is used by the Flemish Environmental Agency (Cabus, 2008), and apply it to a catchment
92 in Flanders, Belgium. The objective of this research is to assess whether the BL stochastically
93 generated rainfall and consistent evapotranspiration time series can be used for hydrological im-
94 pact analyses. In particular, we will evaluate different ways to apply stochastically modelled time
95 series as forcing data to simulate the catchment’s discharge. By regarding the actual observed
96 time series as one realisation of the meteorological process, the corresponding discharge can also

97 be regarded as one realisation. Actually, due to chaos occurring in the climatological system, a
 98 different time series could have been observed resulting in a discharge time series different from the
 99 actual observed one. The latter will hence provide other design values than those corresponding
 100 to the actual observed time series. In order to account for this kind of uncertainty, different cases,
 101 in which the number of stochastically generated input variables to the model is increased, are
 102 investigated. For these cases, the increase of uncertainty in modelled extremes and what portion
 103 of this increase can be attributed to the different stochastic generators, is assessed.

104
 105 Section 2 describes the historical records and all models used within this study. Section 3
 106 briefly introduces the coupled stochastic rainfall-evapotranspiration model and all the considered
 107 situations to simulate discharge from stochastic forcing data. The discharge simulations from dif-
 108 ferent scenarios are then evaluated in Section 4 allowing for assessing the impact of stochastic data
 109 on the simulation of discharge. Finally, conclusions and recommendations are given in Section 5.

110 2 Data and models

111 2.1 Historical data

112 This study uses observed time series measured in the climatological park of the Royal Mete-
 113 orological Institute (RMI) at Uccle, near Brussels, Belgium. The data include time series of
 114 observed precipitation [mm] from 1898–2002, and mean daily temperature T [°C] and daily refer-
 115 ence evapotranspiration E [mm/day] from 1931–2002. The time series of E is derived using the
 116 Penman-Monteith equation. The precipitation data have been recorded with a time resolution
 117 of 10 min from 01/01/1898 to 31/12/2002 measured by a Hellmann–Fuess pluviograph (Démarée,
 118 2003). This data set is quite unique in hydrology due to its extraordinary length with a sampling
 119 frequency of 10 minutes. Its high quality is ensured by using the same method of processing and
 120 measuring at the same location since 1898 (Ntegeka and Willems, 2008). This time series has
 121 been used in several studies (Verhoest et al., 1997; Vaes and Berlamont, 2000; De Jongh et al.,
 122 2006; Ntegeka and Willems, 2008; Vandenberghe et al., 2010; Vanhaute et al., 2012; Pham et al.,
 123 2013; Willems, 2013; Pham et al., 2016) and is used to calibrate the rainfall model as explained
 124 in Section 2.4. This time series has also been reprocessed to daily total precipitation [mm/day],
 125 further referenced to as P , for the period of 1931–2002, which is then used together with the time
 126 series of T and E for the construction of different stochastic models.

127
 128 In order to use the above-described data to fit copulas, the data should be independent and
 129 identically distributed (*iid*), indicating that the distribution of the data should not change with
 130 time. To this end, the time series is split into monthly series to which a vine copula model can be
 131 fitted. Hence, for each month a different model will be obtained. However, the data distributions
 132 can also change within the monthly series, i.e. a within-month trend may exist. Therefore, the
 133 daily distributions, each containing 72 observations, were compared within each month by means
 134 of an ANOVA test when distributions were homoscedastic, a Welch ANOVA test (Welch, 1951)
 135 when distributions were heteroscedastic, or a Kruskal Wallis test (Kruskal and Wallis, 1952) when
 136 distributions were not-normal and heteroscedastic, at a significance level of 0.001. The results
 137 of these tests indicate that within-month trends exist for temperature and evapotranspiration,
 138 whereas no trend was found for precipitation. In order to meet the requirements of the data to
 139 be *iid*, temperature and evapotranspiration data were standardized as follows:

$$x_{s,d,y} = \frac{(x_{d,y} - \mu_d)}{\sigma_d}, \quad (1)$$

140 with $x_{s,d,y}$ the standardized value of temperature or evapotranspiration at day d of year y , $x_{d,y}$
 141 the original measured value of temperature or evapotranspiration at day d of year y , μ_d and σ_d
 142 the mean value and standard deviation of x at day d .

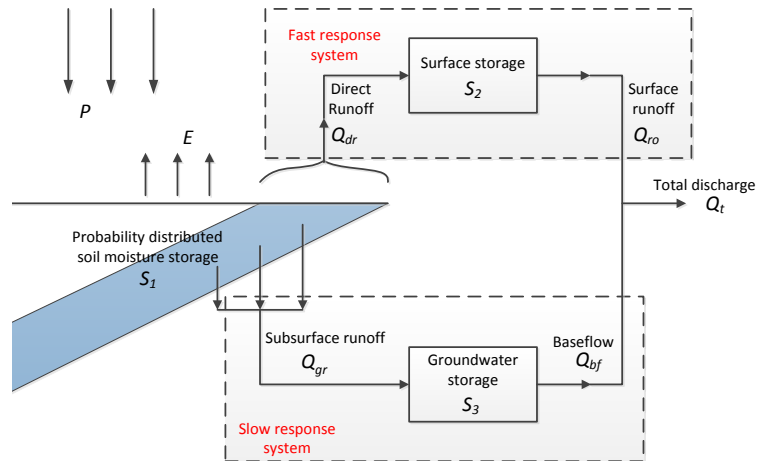


Figure 1: General model structure of the PDM (adapted from Moore, 2007).

143 2.2 Probability Distributed Model (PDM)

144 PDM is a lumped rainfall-runoff model which basically conceptualizes the absorption capacity of
 145 soil in the catchment as a collection of three different storages (Moore, 2007; Cabus, 2008) (see
 146 Fig. 1): i.e. (1) a probability distributed soil moisture storage (S_1) based on a Pareto distribution
 147 of soil moisture capacity to separate direct runoff Q_{dr} and subsurface runoff Q_{gr} ; (2) a surface
 148 storage (S_2) to transform direct runoff into surface runoff; and (3) a groundwater storage (S_3) to
 149 convert subsurface runoff to baseflow. The input for S_1 is the net precipitation ($P - E$), in which
 150 P and E are the precipitation and evapotranspiration, respectively. Further water loss from S_1
 151 may be due to Q_{dr} or Q_{gr} . The former is then converted to surface runoff Q_{ro} through surface
 152 storage S_2 , a fast response system involving a sequence of two linear reservoirs with small storage
 153 time constants k_1 and k_2 . The direct runoff flow only happens for those parts of S_1 that are
 154 completely filled. The recharge to the groundwater, controlled by the drainage time constant k_g ,
 155 is transferred into baseflow Q_{bf} through groundwater storage S_3 , a slow non-linear response system
 156 with a large storage time constant k_b . The sum of Q_{ro} and Q_{bf} equals the total discharge Q_t ;
 157 note that a constant flow which presents any returns or abstractions to or from the catchment,
 158 represented by a parameter q_{const} , also can be added. For a more detailed theoretical explanation
 159 and mathematical description of the model, we refer to Moore (2007).

160
 161 In this study, PDM is calibrated for the Grote Nete catchment using the Particle Swarm Op-
 162 timization algorithm (PSO) (Kennedy and Eberhart, 1995). This catchment, covering about 385
 163 km² in the North of Belgium, has a maritime, temperate climate with an average precipitation of
 164 about 800 mm/year (Vrebos et al., 2014). Given the relatively small distance between Uccle and
 165 the Grote Nete catchment, and the fact that the meteorological conditions are nearly the same, one
 166 can assume that the statistics of the modelled discharge obtained with the forcing data observed
 167 near the catchment and those observed at Uccle are negligible. Furthermore, the rainfall-runoff
 168 model will not be used to make predictions, but rather to demonstrate the impact of different
 169 alternative realisations of precipitation (P), temperature (T) and evapotranspiration (E) on dis-
 170 charge values. Therefore, although PDM will be applied to observations from Uccle in this study,
 171 it is calibrated on the basis of a time series of more than 6 years (from 13/8/2002–31/12/2008)
 172 at an hourly time-step (precipitation, evapotranspiration and discharge) that is available for the
 173 catchment. Observations recorded during the period of 13/8/2002–31/12/2006 are used for model
 174 calibration, while the remaining data (from 1/1/2007–31/12/2008) are used for model validation.
 175

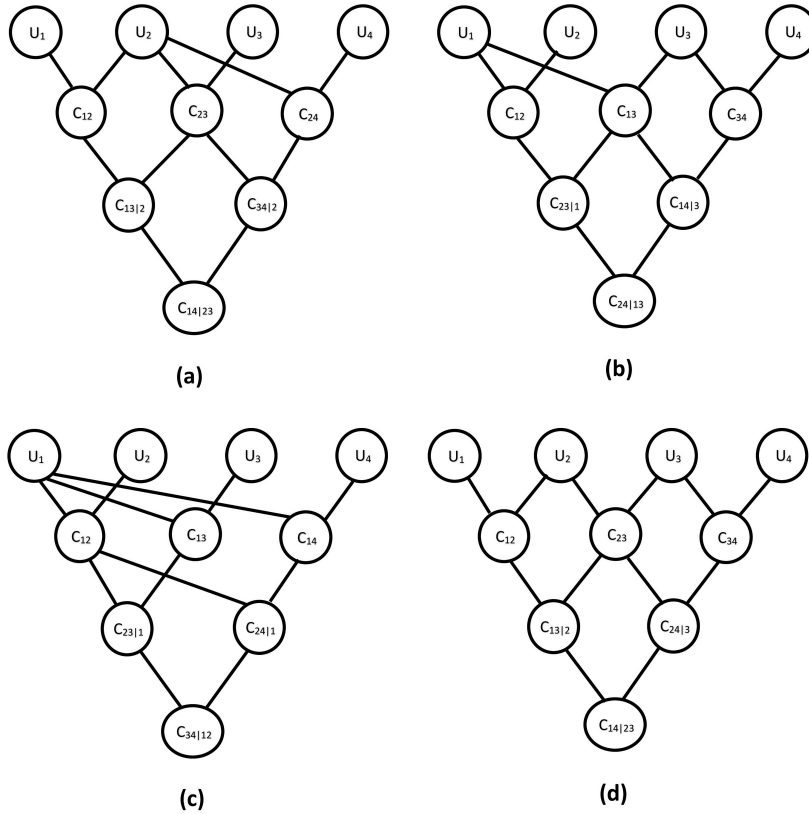


Figure 2: Examples of four-dimensional vine copulas: (a, b) regular vine copulas, (c) canonical vine or C-vine copula, (d) D-vine copula.

2.3 Copula-based stochastic simulation of evapotranspiration and temperature

2.3.1 Vine copulas

A copula is a multivariate function that describes the dependence structure between random variables, independently of their marginal distributions (Sklar, 1959). The theorem of Sklar (Sklar, 1959) states that if $F_{12}(x_1, x_2)$ is the joint distribution function of two random variables X_1 and X_2 with marginal cumulative distributions F_1 and F_2 , then there exists a bivariate copula C_{12} such that:

$$F_{12}(x_1, x_2) = C_{12}(F_1(x_1), F_2(x_2)) = C_{12}(u_1, u_2), \quad (2)$$

with $u_1 = F_1(x_1)$ and $u_2 = F_2(x_2)$. For more theoretical details, we refer to Sklar (1959); Nelsen (2006) and Joe (1997).

The use of copulas allows to decompose the construction of a joint distribution function in two independent steps, i.e. the modelling of the dependence structure and the modelling of the marginal distribution functions (Nelsen, 2006; Salvadori and De Michele, 2007). As such, copulas allow the use of complex marginal distribution functions (Salvadori et al., 2007). Because of this advantage, the application of copulas is becoming more and more popular in hydrological and meteorological studies. However, due to the complication in the construction of the copula model for more than two variables, most research is limited to the bivariate case (Pham et al., 2016).

A flexible construction method for high-dimensional copulas, known as the vine copula construction, has been introduced in the work of Bedford and Cooke (2001, 2002), in which multivariate copulas, and hence the multivariate densities, are constructed as a product of bivariate copula densities. Vine copulas constitute two main advantages. First, they are simple and straightforward

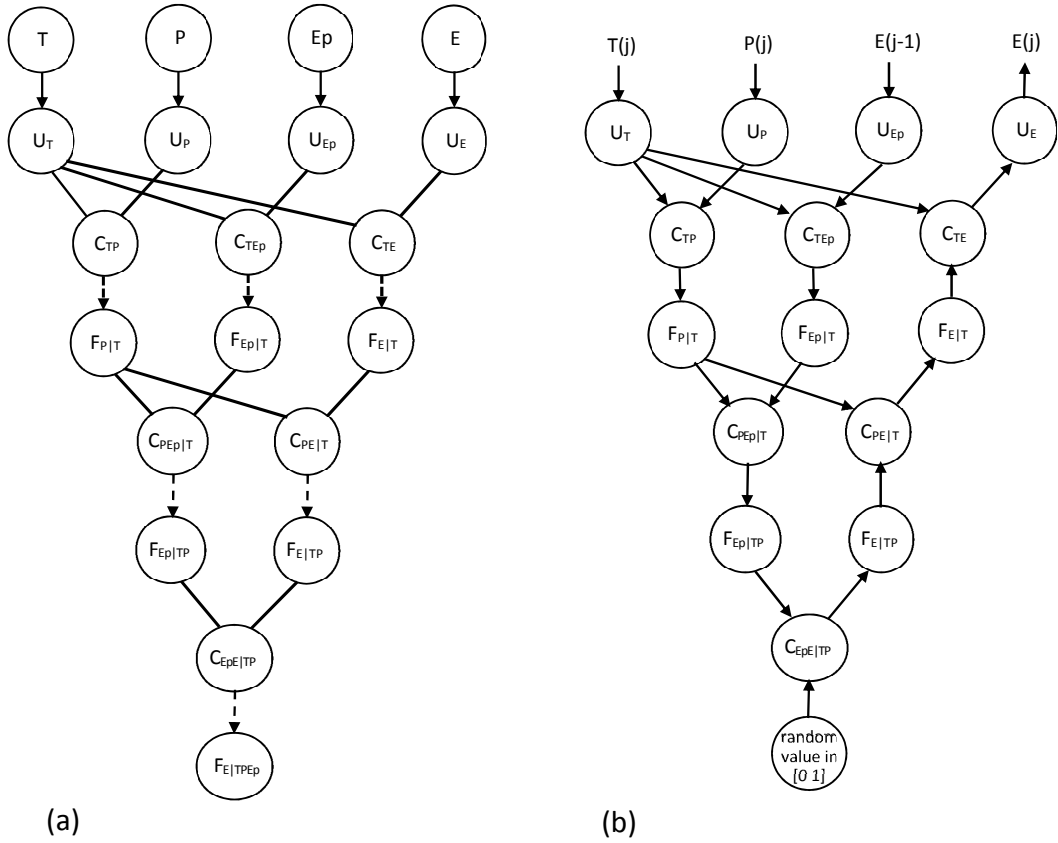


Figure 3: Construction of C-vine copula V_{TPE_pE} (a) and simulation of E from V_{TPE_pE} (b)

199 to apply. Second, they are very flexible and have the ability to model a wide range of dependence
 200 structures because the bivariate copulas can be selected from a large number of copula families
 201 (Kurowicka and Cooke, 2007; Aas et al., 2009; Czado, 2010). However, one has to be aware that
 202 the flexibility offered by vine copulas demands the estimation of a large number of parameters for
 203 which the data set should encompass sufficient information.

204
 205 There is, however, a large number of possibilities for the construction of vine copulas (Aas
 206 et al., 2009); for example, there are 24 and 240 different constructions of vine copulas for the
 207 four- and five-dimensional case, respectively (Aas et al., 2009). Examples of two regular four-
 208 dimensional vine copulas are given in Fig. 2(a, b). One usually focuses on two special types of
 209 regular vine copulas: Canonical vine copulas (C-vine copulas) and D-vine copulas (Kurowicka
 210 and Cooke, 2007). If all mutual dependences involve the same variable, the construction yields a
 211 C-vine copula (Fig. 2(c)). If all mutual dependences are considered one after the other, i.e. the
 212 first with the second, the second with the third, the third with the fourth, etc., the construction
 213 yields a D-vine copula (Fig. 2(d)). In this study, C-vine copulas are used for the constructions of
 214 copula-based generators of temperature and evapotranspiration. More details on the construction
 215 of and simulation from a C-vine copula are given in the work of Aas et al. (2009).

216 2.3.2 Copula-based stochastic simulation of evapotranspiration

217 In order to generate stochastic time series of evapotranspiration, we make use of the vine-copula-
 218 based approach proposed in the work of Pham et al. (2016) in which C-vine copulas are used to
 219 describe the dependences between evapotranspiration and other variables, such as temperature,
 220 precipitation and dry fraction within a day. The advantage of the method is that the statistical
 221 properties of the evapotranspiration time series and the dependence structures between evapo-
 222 transpiration and other variables are well maintained. Furthermore, the model construction and

Table 1: Bivariate copula families selected by AIC for V_{TPE_pE} , where F stands for Frank, Ga for Gaussian, G for Gumbel, C for Clayton, J for Joe and t for t -copula family.

Month	V_{TPE_pE}					
	C_{TP}	C_{TE_p}	C_{TE}	$C_{PE_p T}$	$C_{PE T}$	$C_{E_pE TP}$
Jan	F	F	F	F	F	t
Feb	F	F	F	Ga	Ga	t
Mar	C	t	t	Ga	F	t
Apr	Ga	G	G	F	F	G
May	F	G	G	F	F	t
Jun	F	G	Ga	F	F	t
Jul	F	G	Ga	F	F	G
Aug	F	G	Ga	t	F	G
Sep	Ga	Ga	G	F	F	t
Oct	C	G	G	F	F	t
Nov	C	t	t	Ga	Ga	t
Dec	F	F	F	F	Ga	t

simulation are simple to apply. After comparing the results of different vine models, Pham et al. (2016) found that the best simulations of daily evapotranspiration were provided by the four-dimensional C-vine copula V_{TPDE} relating daily temperature (T), precipitation (P), dry fraction (D) and evapotranspiration (E), and the three-dimensional C-vine copula V_{TPE} relating T , P and E . As there is no major difference in performance between simulations using V_{TPDE} and V_{TPE} (Pham et al., 2016), for simplicity, we choose to use only temperature, precipitation and evapotranspiration data in the vine copula model for evapotranspiration. In order to avoid monthly effects, the temperature and evapotranspiration data were first standardized and a different C-vine copula model is used for each month. However, subsequent observations of the time series may not be independent, meaning that values within the time series may be autocorrelated. This is accounted for by extending the vine copula V_{TPE} as used in Pham et al. (2016) with the evapotranspiration of the previous day (E_p). In this way a four-dimensional C-vine copula V_{TPE_pE} is constructed for each month. The best bivariate copula families for the C-vine copulas are chosen using Akaike's information criterion (AIC) (Akaike, 1973) from five one-parameter copula families, i.e. the Gaussian, the Gumbel, the Frank, the Joe and the Clayton family and one two-parameter family, the t -copula family. Table 1 lists the selected copula families. The empirical cumulative distribution functions are used as marginal distributions, and the final copula parameters of the one-parameter families are determined on the basis of the relationship between the copula parameter and Kendall's tau, whereas the parameters of the t -copula family are estimated through maximum likelihood estimation.

Further, the White goodness-of-fit test (Schepsmeier, 2015) is applied to check whether the dependence present in the data is captured by the C-vine copulas. For this test, p -values larger than the significance level indicate that the dependence structure of the data can be described by the selected copulas. In this study, all but one p -value were larger than the used significance level of 0.05. The dependence structure of the data can thus be described by the selected copula families.

The construction of V_{TPE_pE} is given as follows (see Fig. 3(a)). First, values ($u_{T,j}, u_{P,j}, u_{E_p,j}, u_{E,j}$) of U_T, U_P, U_{E_p} and U_E are derived from the marginal distributions of respectively T, P, E_p and E ($j = 1, \dots, n$ and n is the number of data points), and are used to select and fit the bivariate copulas C_{TP}, C_{TE_p} and C_{TE} . These bivariate copulas are conditioned on U_T through partial differentiation as given in Eq. (3), resulting in the conditional cumulative distribution functions

255 $F_{P|T}$, $F_{E_p|T}$ and $F_{E|T}$.

$$\begin{aligned}
F_{P|T}(u_P|u_T) &= \frac{\partial}{\partial u_T} C_{TP}(u_T, u_P), \\
F_{E_p|T}(u_{E_p}|u_T) &= \frac{\partial}{\partial u_T} C_{TE_p}(u_T, u_{E_p}), \\
F_{E|T}(u_E|u_T) &= \frac{\partial}{\partial u_T} C_{TE}(u_T, u_E).
\end{aligned} \tag{3}$$

256 Using these three conditional distributions, the conditional probabilities are calculated for all
257 data points $(u_{T,j}, u_{P,j}, u_{E_p,j}, u_{E,j})$. To these conditional probabilities, which are also uniformly
258 distributed on $[0,1]$, two bivariate copulas $C_{PE_p|T}(F_{P|T}, F_{E_p|T})$ and $C_{PE|T}(F_{P|T}, F_{E|T})$ are fitted,
259 of which the partial derivatives to $F_{P|T}$ can be computed to obtain $F_{E_p|TP}$ and $F_{E|TP}$. Again,
260 using these two conditional distributions, a bivariate copula $C_{E_pE|TP}(F_{E_p|TP}, F_{E|TP})$ is fitted,
261 which can also be conditioned by calculating the partial derivative. For more detailed information
262 about the construction of vine copulas, we refer to (Aas et al., 2009). Once the C-vine copula
263 model is fitted, a corresponding time series of evapotranspiration values can be generated, for a
264 given time series of rainfall and temperature data, by sampling the copula (Fig. 3(b)). To that
265 end, values of U_E are calculated as:

$$u_E = F_{E|T}^{-1}(F_{E|TP}^{-1}(F_{E|TPE_p}(r|u_T, u_P, u_{E_p}))), \tag{4}$$

266 where r is a random value drawn from a uniform distribution on $[0,1]$. Then the corresponding
267 evapotranspiration value e can be calculated using the inverse marginal distribution function:

$$e = F_E^{-1}(u_E). \tag{5}$$

268 It is clear that the values of U_E are affected by the random value r , therefore, several simulations
269 will show some variability. To account for these stochastic effects, the simulation was repeated
270 50 times. Figure 4 displays the comparisons between probability density functions of observed
271 and simulated evapotranspiration obtained by V_{TPE_pE} for the different months. From these plots,
272 it can be seen that the probability density functions of the stochastic evapotranspiration are
273 very similar to those of the reference evapotranspiration in Uccle (red line). In order to assess
274 whether the dependence structures between simulated evapotranspiration and other variables are
275 maintained, for each of the 50 simulations, the mutual dependences between E and the other
276 variables, T or P , were assessed via Kendall's tau for each month. Figure 5 shows box plots of the
277 obtained values of Kendall's tau for E vs. T and E vs. P dependences for 50 simulations. These
278 figures show that, in general, the observed dependences between both E vs. T and E vs. P
279 are preserved with the stochastic simulated evapotranspiration.

280 2.3.3 Copula-based stochastic simulation of temperature

281 Temperature data are required for the stochastic modelling of evapotranspiration. However, in
282 situations where no long-term time series of temperature is available, it is necessary to use a
283 stochastically generated temperature time series. We use a similar approach as Pham et al.
284 (2016) to develop a stochastic temperature model based on copulas. This model makes use of the
285 dependence between the temperature and the precipitation of the same day (i.e. at day j) and the
286 temperature of the previous day (i.e. at day $j-1$). Similarly as for the stochastic evapotranspiration
287 model, a C-vine copula is employed in which T_{j-1} is chosen as the core variable. The model
288 is referred to as V_{T_pPT} , where T_p refers to the temperature of the previous day.

289
290 The construction procedure of V_{T_pPT} is similar to the one of V_{TPE_pE} with that difference that
291 only 3 instead of 6 bivariate copulas need to be fitted (see Section 2.3.2). The simulation process
292 of the temperature model is different from that of the evapotranspiration model, in the sense that
293 it requires a modelled input from the previous time step (i.e. T_p) in order to generate a new value
294 for T . The simulation algorithm of T can be performed as follows:

Table 2: Bivariate copula families selected by AIC for V_{T_pPT} , where F stands for Frank, Ga for Gaussian, G for Gumbel, C for Clayton, J for Joe and t for t -copula.

Month	V_{T_pPT}		
	C_{T_pP}	C_{T_pT}	$C_{PT T_p}$
Jan	F	t	F
Feb	F	t	F
Mar	F	t	F
Apr	F	Ga	F
May	F	t	F
Jun	F	Ga	F
Jul	F	Ga	F
Aug	F	Ga	F
Sep	Ga	t	t
Oct	C	t	C
Nov	C	t	F
Dec	F	t	F

$$u_T = F_{T|T_p}^{-1}(F_{T|T_pP}^{-1}(r|u_{T_p}, u_P)), \quad (6)$$

$$t = F_T^{-1}(u_T). \quad (7)$$

295 Similarly as for the evapotranspiration model, the best bivariate copula families for the C-vine
 296 copulas are chosen using the AIC. Table 2 illustrates which copula families were selected. This
 297 table shows that the Frank copula family is often selected for C_{T_pP} and $C_{PT|T_p}$, while the Gaussian
 298 and the t -copula are often chosen for C_{T_pT} . Further, the White goodness-of-fit test (Schepsmeier,
 299 2015) is also applied to check whether the dependence present in the data is captured by the
 300 C-vine copulas. All p -values were larger than the used significance level of 0.05, indicating that
 301 the dependence structure of the data can be described by the selected copula families. The final
 302 copula parameters of the one-parameter families are determined on the basis of the relationship
 303 between the copula parameter and Kendall's tau, whereas the parameters of the t -copula family
 304 are estimated through maximum likelihood estimation. These copulas are then used for generating
 305 temperature given the time series of precipitation.

306
 307 To assess the performance of the model, the statistics of 50 stochastic time series of temperature
 308 using the observed daily precipitation from 1931 to 2002 are compared to those of the observations.
 309 The empirical probability density functions of the monthly mean temperature for each of the
 310 simulated 72-year time series are shown in Fig. 6. The statistics of the simulations seem to be
 311 relatively similar to the observations. Figure 7 shows the monthly maximum temperature of the
 312 ensemble and of the observed temperature series corresponding to their empirical return periods.
 313 This figure shows that the extremes are well modelled for all months.

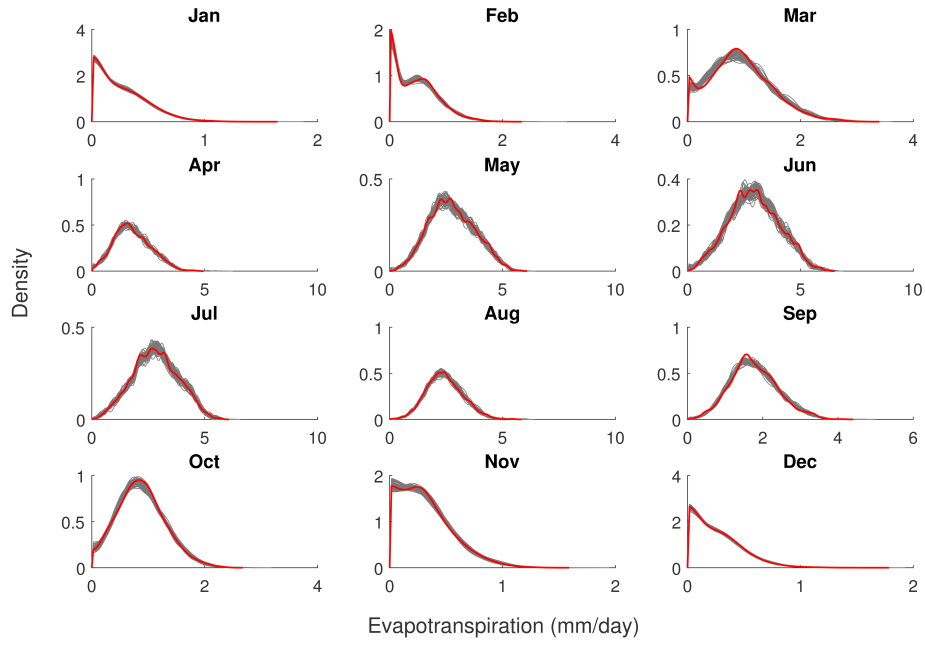


Figure 4: Comparison between the probability density functions of evapotranspiration of observed and simulated values: Uccle (red), the ensemble of 50 time series simulated using the C-vine copula V_{TPE_pE} (grey).

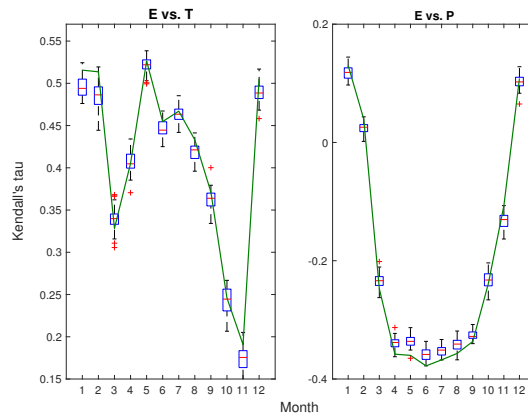


Figure 5: Comparison between Kendall's tau for the relations of E vs. T (left) and E vs. P (right) of observed and simulated values: Uccle (green line), 50 simulated time series (box plot).

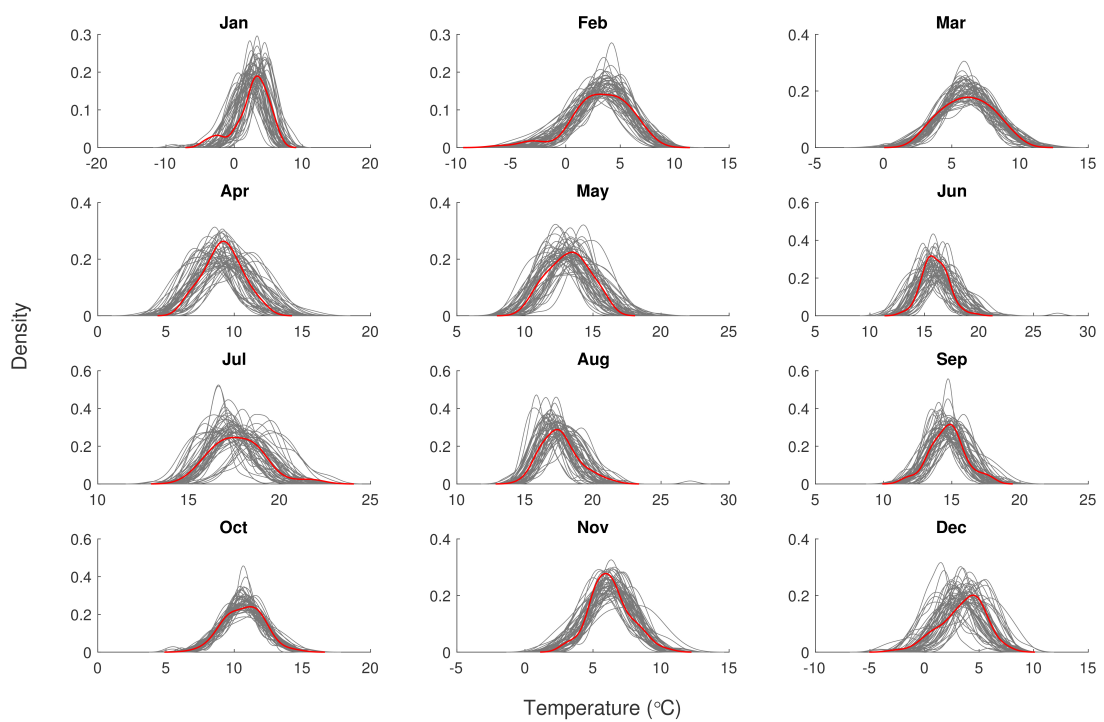


Figure 6: Comparison between the probability density functions of the monthly mean T of the observed and simulated values: Uccle (red), the ensemble of 50 time series simulated using the C-vine copula V_{TPPT} (grey).

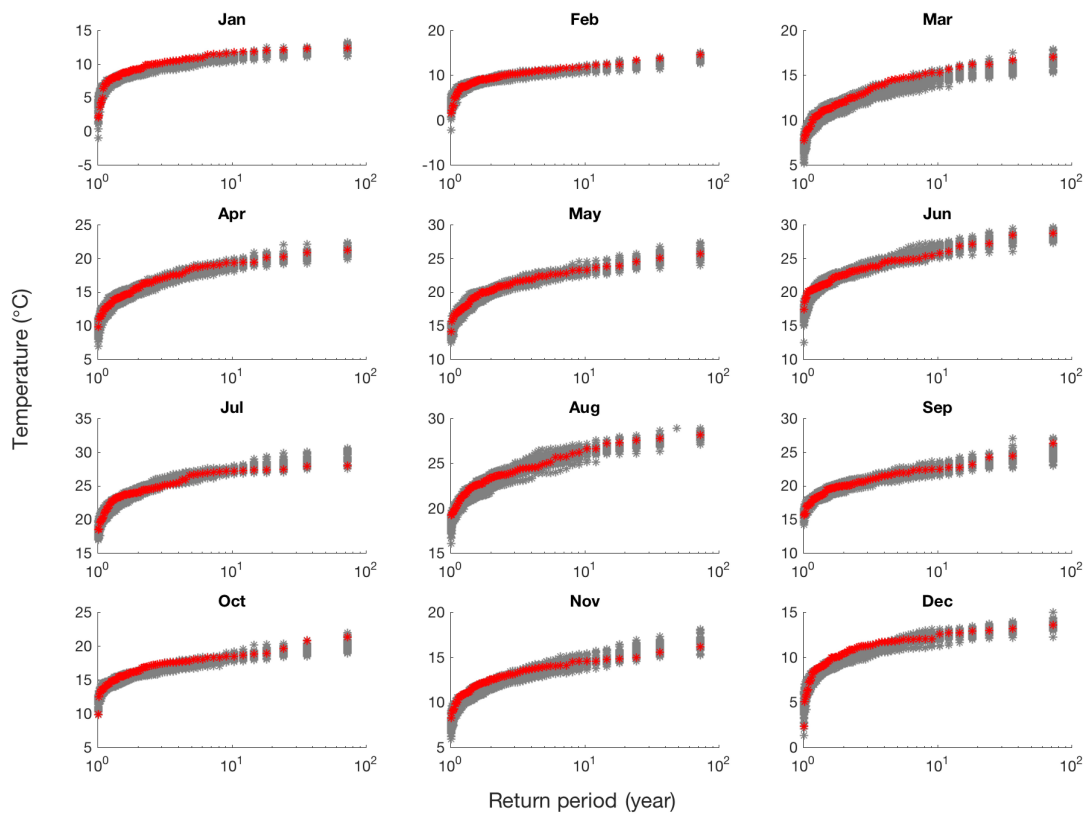


Figure 7: Comparison between the return periods of monthly extremes of the observed and simulated temperature values: Uccle (red), the ensemble of 50 time series simulated using the C-vine copula V_{TPPT} (grey).

Table 3: Optimal parameter set for the (monthly) MBL model.

Parameter	λ	κ	ϕ	μ_x	α	ν
January	0.021	0.009	0.002	11.037	12.042	0.833
February	0.014	0.008	0.001	15.000	4.041	0.143
March	0.018	0.009	0.001	15.000	5.393	0.219
April	0.017	0.151	0.032	0.823	20.000	19.029
May	0.023	1.130	1.000	0.371	4.000	14.420
June	0.016	0.089	0.059	1.190	10.064	20.000
July	0.012	0.012	0.004	7.676	20.000	5.715
August	0.010	0.003	0.001	15.000	19.963	2.729
September	0.014	0.199	0.100	0.417	4.000	14.039
October	0.013	8.949	0.096	0.095	4.000	2.488
November	0.023	0.121	0.026	1.061	4.000	2.486
December	0.014	0.005	0.001	14.998	20.000	1.792

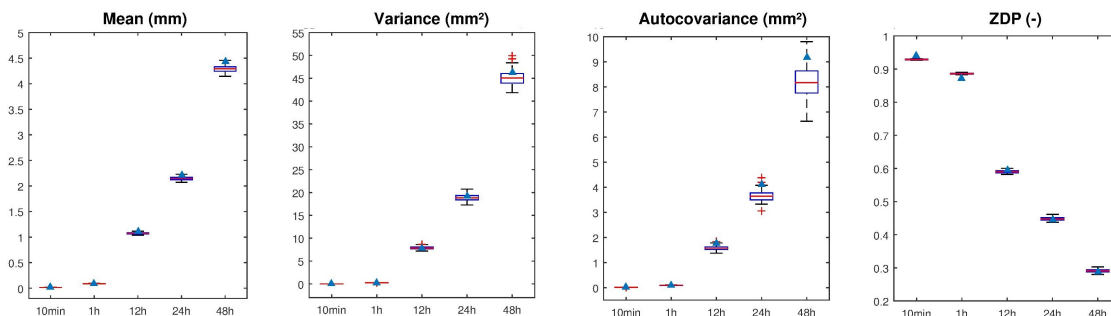


Figure 8: Comparison between observed and simulated precipitation data for the mean, variance, autocovariance and zero-depth probability (ZDP): Uccle (blue triangle), the ensemble of 50 simulated time series by the MBL model (box plot).

2.4 Simulated precipitation by the MBL model

In situations where no long time series of precipitation is available, one can use a stochastic rainfall model. In this study, the modified Bartlett–Lewis (MBL) model (Rodriguez-Iturbe et al., 1988) is selected to generate the precipitation time series based on the results from Pham et al. (2013) in which the MBL model is considered to be the best version of the different BL models tested on the Uccle data set. The MBL model is calibrated using the Generalised Method of Moments, i.e. the difference between the model statistics obtained by means of analytical expressions and the empirical statistics obtained from the observed time series is to be minimized. The calibration of the MBL model in this study is based on the mean, variance, lag-1 autocovariance and zero-depth probability (ZDP) at the aggregation levels of 24 h, 48 h and 72 h instead of 10 min, 1 h and 24 h that were used in Pham et al. (2013). As in Pham et al. (2013), the Shuffled Complex Evolution algorithm (Duan et al., 1994) was employed to search for the optimal parameters. The reason for only selecting aggregation levels of at least one day is to consider situations where only daily precipitation data would be available. The values of the calibrated parameters are given in Table 3. Details of the MBL model and the model calibration are provided by Pham et al. (2013) and Vanhaute et al. (2012). The stochastic rainfall time series is simulated at the same 10-minute time resolution as the observations. In order to assess the performance of the model, the abilities of the model to reproduce some general historical statistics, such as mean, variance, the lag-1 autocovariance and ZDP, at aggregation levels of 10 min, 1 h, 12 h, 24 h and 48 h are investigated based on an ensemble of 50 time series.

In Fig. 8, some general statistics at different aggregation levels are compared for 50 time series obtained by the MBL model and the observed time series in Uccle. In order to further unveil the behaviour of the model, the general statistics are calculated at different aggregation levels for

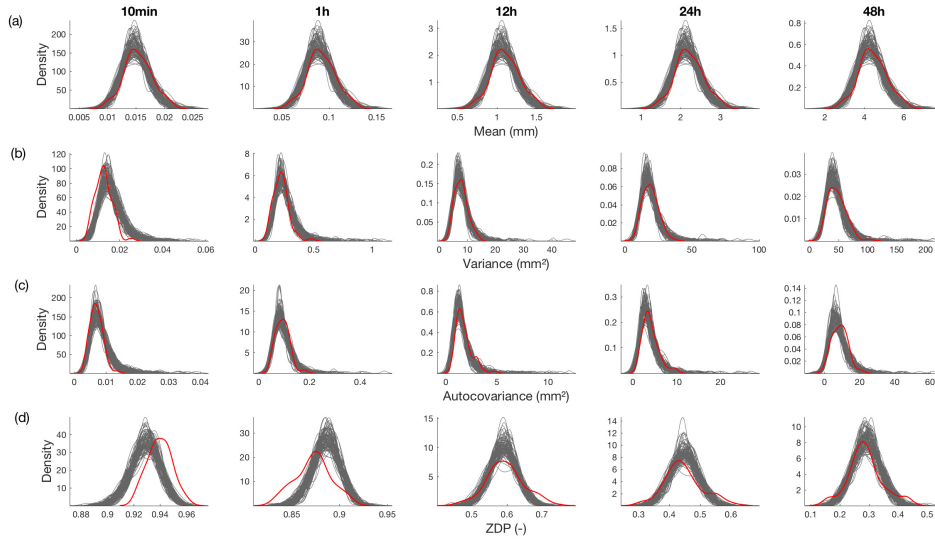


Figure 9: Comparisons between the probability density functions of mean, variance, autocovariance and ZDP calculated for the observed and simulated precipitation data for different aggregation levels for each year: Uccle (red), 50 simulated time series by the MBL model (grey). Densities are shown for the (a) mean, (b) variance, (c) lag-1 autocovariance and (d) the zero-depth probability (ZDP).

338 each year and presented in the form of a frequency distribution (Fig. 9). From both figures, it
 339 can be seen that the mean is generally reproduced well by the model at all levels of aggregation.
 340 At the sub-hourly level, the variance and autocovariance are slightly overestimated. For higher
 341 aggregation levels, an increasing variation is found for both statistical properties. At higher levels
 342 of aggregation, the ZDP is relatively similar to that found for the observed time series, whereas
 343 for hourly and sub-hourly levels, a slight deviation in ZDP-values are found with respect to the
 344 observations.

345

346 Figure 10 shows the empirical univariate return periods of the annual maximum rainfall depths
 347 of the observed and simulated series, considering five different aggregation levels. Compared to the
 348 observations, it seems that the MBL model is able to preserve the maxima at all aggregation levels.
 349 It can be seen in this study that the MBL model does not suffer from the problem of underestima-
 350 tion of extreme values at sub-hourly aggregation levels that were reported in the work of Verhoest
 351 et al. (1997) and Cameron et al. (2000). From the analysis, it seems that the MBL model is
 352 capable of preserving the sub-daily statistics even though the calibration procedure only included
 353 daily and multi-day statistics. Yet, further research is needed for exploring this improved behavior.

354

355 Figure 10 also shows that a large variation in extreme values is found for larger return periods.
 356 The MBL model allows for generating rainfall time series mimicking the statistics of the observed
 357 series. Due to its structure, the modeled precipitation values are not restricted to the range of
 358 rainfall values in the observations, making this model able to generate rainfall events having a
 359 return period larger than the observed time series. Yet, it can thus be expected that within
 360 the modeled time series of 72 years, events may occur having a true return period that is larger
 361 than the length of the modeled time series. If longer time series would be simulated, a better
 362 estimation of the rainfall corresponding to return periods that are smaller than the observed time
 363 series should be obtained. To demonstrate this, all 50 series generated are concatenated, resulting
 364 in one time series of $50 \times 72 = 3600$ years, for which the return periods are calculated empirically
 365 and plotted (only for return periods less than 100 years) as a blue line in Fig. 10. As can be seen
 366 for return periods smaller than 100 years, a good fit with the observations are obtained, showing
 367 that MBL is capable of reproducing extremes. Yet, the user should use much longer time series
 368 than the maximum return period aimed for.

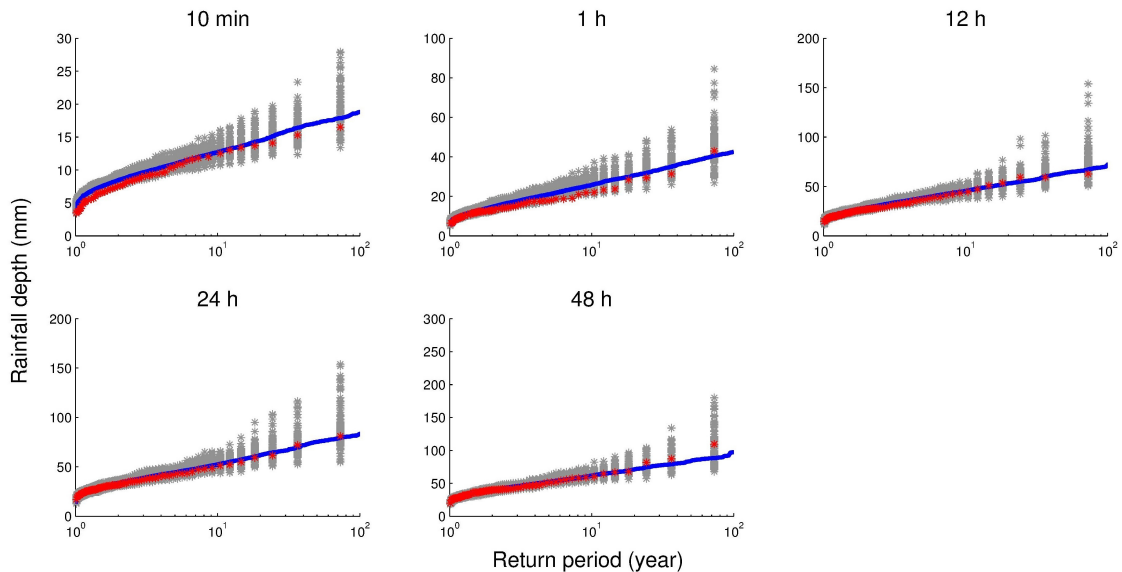


Figure 10: Comparisons between the return periods of extremes of the observed and simulated precipitation data at different aggregation levels: Uccle (red), the ensemble of 50 simulated time series by the MBL model (grey). Calculation of the extremes for a given return period on a time series that is based on concatenating the 50 simulated time series, results in the blue line

3 Discharge simulation scenarios

The catchment discharge is calculated by the PDM that uses precipitation and evapotranspiration data as inputs. In order to assess the impact of each stochastic variable on the modelling of discharge, three cases have been developed that can be compared to a reference situation (cfr. Fig. 11). The reference situation is obtained by running the PDM with the observed time series of precipitation and evapotranspiration. In case 1, it is supposed that insufficient evapotranspiration data would be available (e.g. a shorter time series than the observed precipitation), the stochastic evapotranspiration can then be generated using the three-dimensional C-vine copula, i.e. V_{TPE_pE} , given observed rainfall and temperature. The simulation is repeated 50 times in order to account for stochastic effects. In case 2, where only a sufficient long time series of precipitation is available, the process starts with temperature simulations, then evapotranspiration can be modelled using the observed precipitation and stochastically generated temperature using the V_{TPE_pE} copula. As presented before, temperature values will be generated by the three-dimensional C-vine copula V_{T_pPT} that relates temperature T to daily precipitation P and the daily temperature of the previous day T_p . To account for stochastic effect, 50 time series of temperature are generated. Next, each of 50 time series of temperature, together with the observed precipitation data, are used to simulate 50 corresponding time series of evapotranspiration. Therefore, in total 2500 time series of evapotranspiration are generated. Case 3 accounts for a situation in which data would insufficiently be available for all input variables. In this case, an ensemble of 50 time series of precipitation could be generated using the MBL model. For each of these time series, 50 time series of temperature and 2500 time series of evapotranspiration can be obtained using the same approach in case 2. In total, 125000 time series of evapotranspiration are generated in case 3. In order to construct copula models and evaluate discharge simulations in all cases, this study uses the same time series of precipitation, evapotranspiration and temperature at Uccle. In all cases, discharge is simulated using the PDM that was calibrated for the Grote Nete catchment in Belgium (see Section 2.2). By this approach, the uncertainty due to the PDM can be partly excluded from the study, i.e. we study the change in performance with respect to the reference situation. It makes sense because the three cases use exactly the same PDM, a similar uncertainty due to the model is assumed for all cases as for the reference situation. Therefore, the change in performance for all cases with respect to the reference situation can be attributed to the differences in inputs to the model. The discharge simulations in the three cases are denoted as Q_{s1} , Q_{s2} and Q_{s3} ,

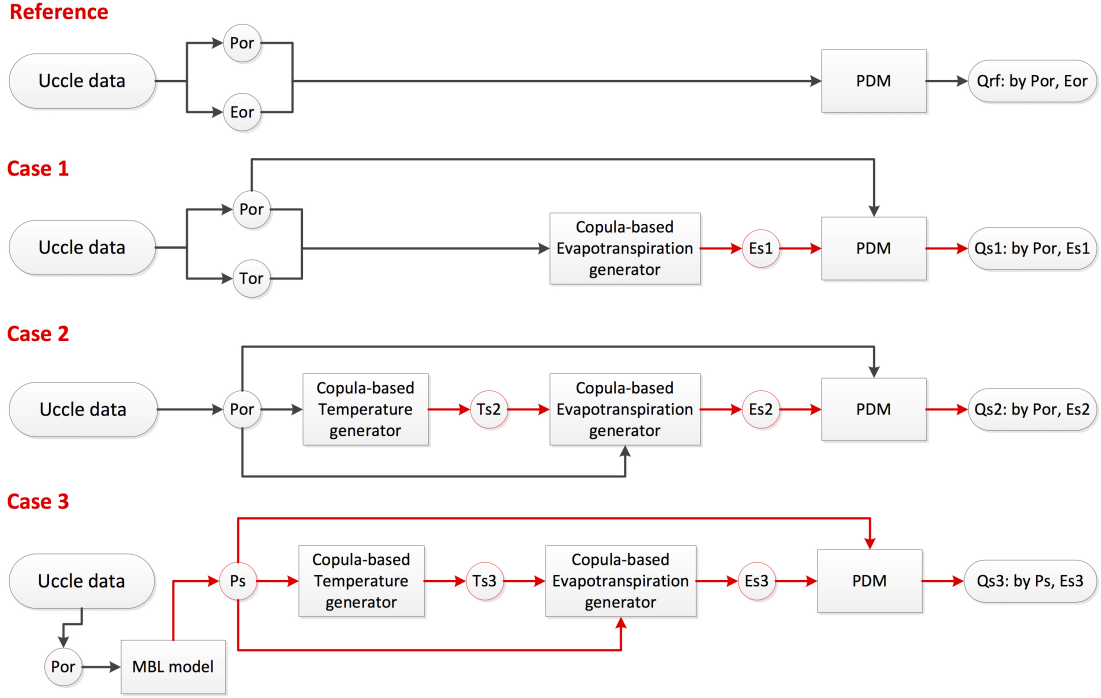


Figure 11: Different cases for discharge simulation. P_{or} , E_{or} and T_{or} refer to the observed time series. P_s , E_{s1} , E_{s2} , E_{s3} , T_{s2} and T_{s3} refer to the simulated time series (red block). Red arrows indicate the simulation processes related to stochastically generated time series.

400 respectively, while the reference discharge is denoted by Q_{rf} .

401 4 Results and discussions

402 4.1 Case 1

403 The catchment discharge can be simulated by means of the PDM that uses precipitation and
 404 evapotranspiration data. In case 1 (cfr. Fig. 11), where only daily observed precipitation and
 405 temperature data are available, 50 stochastically generated evapotranspiration time series are
 406 generated using the three-dimensional C-vine copula V_{TPE_pE} . The results shown in Section 2.3.2
 407 and the work of Pham et al. (2016) reflect that the C-vine copula V_{TPE_pE} performs well and its
 408 simulations lie very close to the values of the observed evapotranspiration. The left panel of Fig. 12
 409 displays the comparison between the probability density functions of Q_{rf} and Q_{s1} for January,
 410 April, July and October. It can be seen that the distributions of Q_{s1} are quite similar to those of
 411 the reference discharge for these months. Similar results are obtained for the other months. For
 412 a further analysis of mean discharges and annual extremes of Q_{s1} , we refer to Section 4.3.

413 4.2 Case 2

414 In case 2 (cfr. Fig. 11), only a time series of precipitation of sufficient length is available and the
 415 temperature values are simulated using the C-vine copula V_{T_pPT} . The observed precipitation and
 416 stochastically generated temperature values are then used for reproducing the evapotranspiration
 417 by means of the C-vine copula V_{TPE_pE} . Through comparing the results of this case with that of
 418 case 1, we can assess the impact of introducing a stochastic temperature model on the modelled
 419 evapotranspiration time series and the modelled discharge.

420
 421 As shown in Section 2.3.3 and Fig. 13 (left panel), the stochastically generated temperature
 422 data generated by the C-vine copula V_{T_pPT} model are reliable and can be used together with
 423 the recorded precipitation to simulate 2500 time series of evapotranspiration in the next step

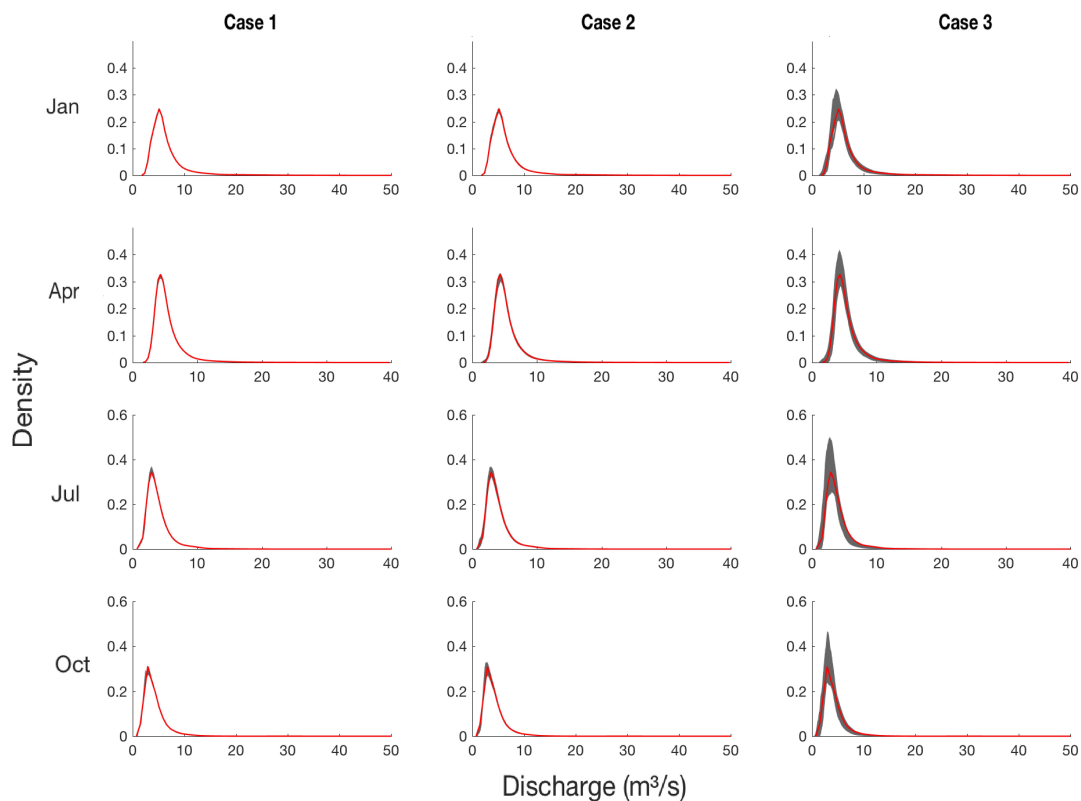


Figure 12: Comparison between the probability density functions of the reference discharge Q_{rf} (red) and the ensemble of time series of simulated discharge values (grey) using observed precipitation, observed temperature and simulated evapotranspiration values in case 1 (left panel), using observed precipitation and simulated temperature and evapotranspiration in case 2 (middle panel) and using simulated precipitation, temperature and evapotranspiration in case 3 (right panel).

424 (i.e. for each temperature series, 50 evapotranspiration series are generated). The probability
 425 density functions of the 2500 time series of the simulated evapotranspiration are shown in Fig. 14
 426 (middle panel). It can be seen from the figures that these distributions are similar to those of
 427 the observations in Uccle and those of the modelled evapotranspiration in case 1 (cfr. Fig. 14
 428 (left panel) for January, April, July and October.) Similar results are obtained for the other
 429 months. Figure 12 (middle panel) displays a comparison between the probability density functions
 430 of the simulated discharge (Q_{s2}) and the reference discharge (Q_{rf}). In general, the grey areas
 431 representing 2500 simulated time series are slightly wider than those in case 1 (Fig. 12 (left
 432 panel)). We conclude that the introduction of stochastically generated temperature does not
 433 cause considerable deviations in the simulation of evapotranspiration and discharge.

434 4.3 Case 3

435 This case accounts for a situation in which no time series (of sufficient length) are available as
 436 shown in Fig. 11. The first step consists of generating 50 time series of precipitation by means of
 437 the MBL model (see Section 2.4) and aggregating these to the daily level. Then, each of those time
 438 series is used for modelling 50 time series of temperature, each used for generating 50 evapotranspi-
 439 ration series. Therefore, in total 125000 time series of evapotranspiration are generated. Finally,
 440 125000 time series of the catchment discharge are simulated using the stochastically generated
 441 time series of precipitation and corresponding evapotranspiration values. This case will allow for
 442 assessing the uncertainty introduced by using the MBL model for generating precipitation values
 443 as input to a rainfall-runoff model.

444
 445

First, the simulated time series of precipitation are used as inputs to the C-vine copula $V_{T_p, PT}$ to

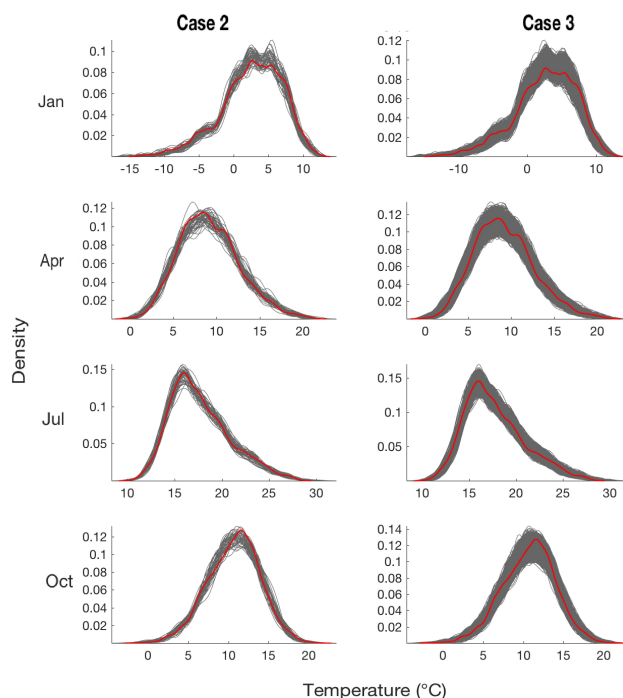


Figure 13: Comparison between the probability density functions of observed temperature time series (red) and the ensemble of simulated time series of temperature values (grey) using the C-vine copula $V_{T_p, PT}$ on the basis of observed precipitation in case 2 (left panel) and on the basis of simulated precipitation in case 3 (right panel).

446 generate time series of temperature. The modelled copula-based temperature values are compared
 447 with the observed temperature in Uccle in terms of the probability density functions in Fig. 13
 448 (right panel). From these figures, it can again be seen that the distributions of the simulations
 449 follow those of the observations. With respect to the probability density functions, the simulated
 450 evapotranspiration (Fig. 14 (right panel)) in this case is similar to the observed evapotranspiration,
 451 but more deviations can be observed in this case than in the previous cases. The modelled
 452 time series of precipitation and evapotranspiration are then used for modelling the discharge. The
 453 probability density functions of the simulated discharge values for some months are displayed in
 454 Fig. 12 (right panel). Similar results are obtained for the other months. From the different plots,
 455 it can be concluded that the simulations still follow the distribution of the reference discharge (red
 456 line).

457

458 Compared to the simulated discharge of cases 1 and 2, more higher extreme values are generated
 459 and the grey areas representing the ensemble of 125000 time series are generally wider, indicating
 460 that mainly the stochastic generation of precipitation has introduced considerable variations into
 461 the discharge simulations. The top panel of Fig. 15 illustrates this by comparing the annual
 462 extremes of the observed and the simulated discharge series for all cases. However, it should also
 463 be noted that the results for cases 2 and 3 are obtained on the basis of a wider ensemble of time
 464 series as compared to case 1 (2500 for case 2, and 125000 for case 3). In order to also compare
 465 the variations obtained on the basis of an equal number of time series within the ensemble (i.e.
 466 50 time series), for each time series of observed (case 2) or simulated (case 3) precipitation,
 467 one corresponding time series of temperature and one corresponding time series of evapotranspiration
 468 are generated. The bottom panel of Fig. 15 illustrates the extremes obtained on the basis of
 469 this ensemble of 50 time series of discharge. These results also show that most of the variation
 470 obtained in case 3 is due to the stochastic generation of precipitation. This increase in uncertainty
 471 should however be treated with care. As stated before, the generated rainfall series may include
 472 extremes that are larger than the ones in the observed time series. Such large precipitation values

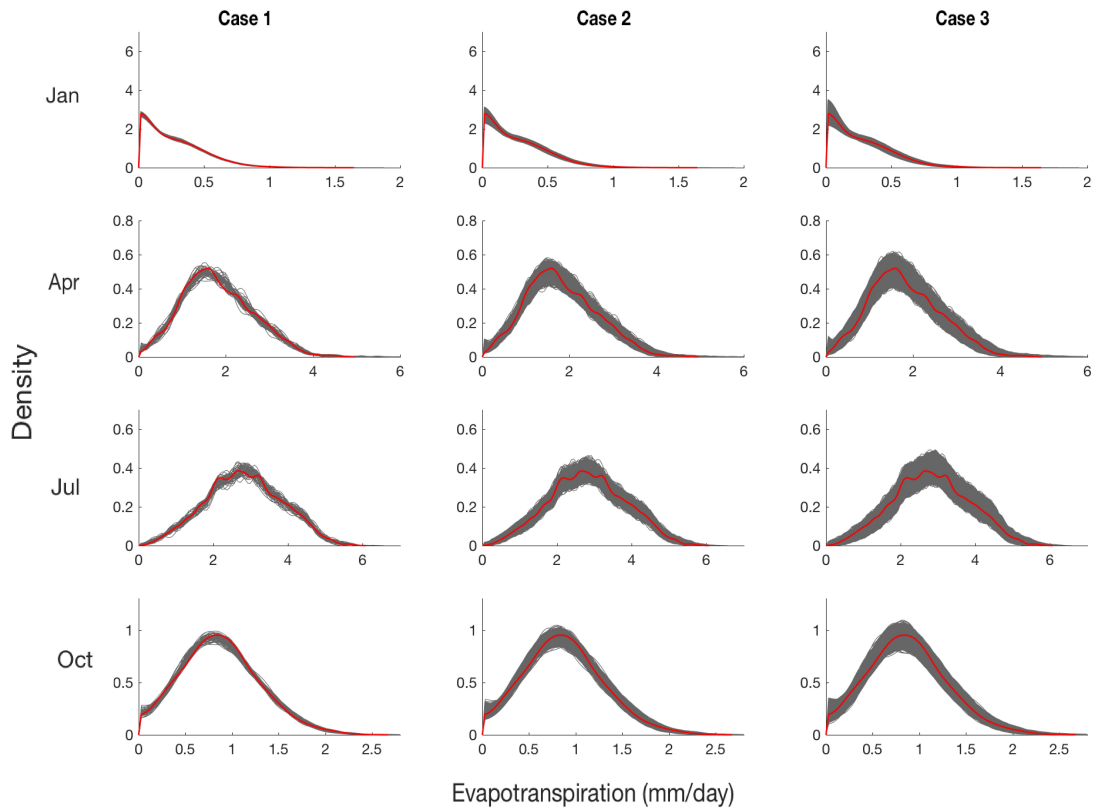


Figure 14: Comparison between the probability density functions of observed evapotranspiration time series (red) and the ensemble of simulated time series of evapotranspiration (grey) using the C-vine copula V_{TPE_pE} on the basis of observed precipitation, observed temperature in case 1 (left panel), on the basis of observed precipitation and simulated temperature in case 2 (middle panel) and on the basis of simulated precipitation and temperature in case 3 (right panel).

473 will inevitably result in a large surface runoff production causing extreme discharges. The large
474 variability in extreme rainfall as observed in Fig. 10 will consequently lead to large variabilities in
475 modeled extreme discharges (cfr. Fig. 15). If, however, the discharge extremes from a longer time
476 series are studied, the variation in extremes is strongly reduced. To demonstrate this, 50 rainfall
477 time series of 3600 year and corresponding evapotranspiration time series (remark that only one
478 series is generated per rainfall time series) are used as input to the rainfall-runoff model, and the
479 extremes, having return periods smaller than 1000 years, are plotted for each of these 50 time series
480 (Fig. 16). As can be seen, the large uncertainties in extremes, encountered when using 72 year
481 time series as input, are highly reduced, showing a slight overestimation for larger return periods,
482 if compared to those modeled using the observed time series of rainfall and evapotranspiration.
483 Yet, it is impossible to state whether true overestimations are obtained, or that, due to the
484 stochastic nature of rainfall (and evapotranspiration), no discharge events corresponding to a 72-
485 year return period occurred in the observed time series and therefore the maximum discharge
486 value was wrongly assigned a too high return period (i.e. the maximum discharge based on the
487 observed time series of precipitation and evapotranspiration corresponds to a return period of
488 about 25 years based on the simulations using the modelled very long time series of precipitation
489 and evaporation). Similarly as discussed for Fig. 10, this result makes a plea for using modeled
490 discharge time series of a length that is a multiple of the maximum return period of discharge
491 aimed at, where longer time series reduce the variation in discharge values at high return periods
492 at the expense of run-time. Further research will be needed to seek for the trade-off between
493 length of the time series and the remaining uncertainty.

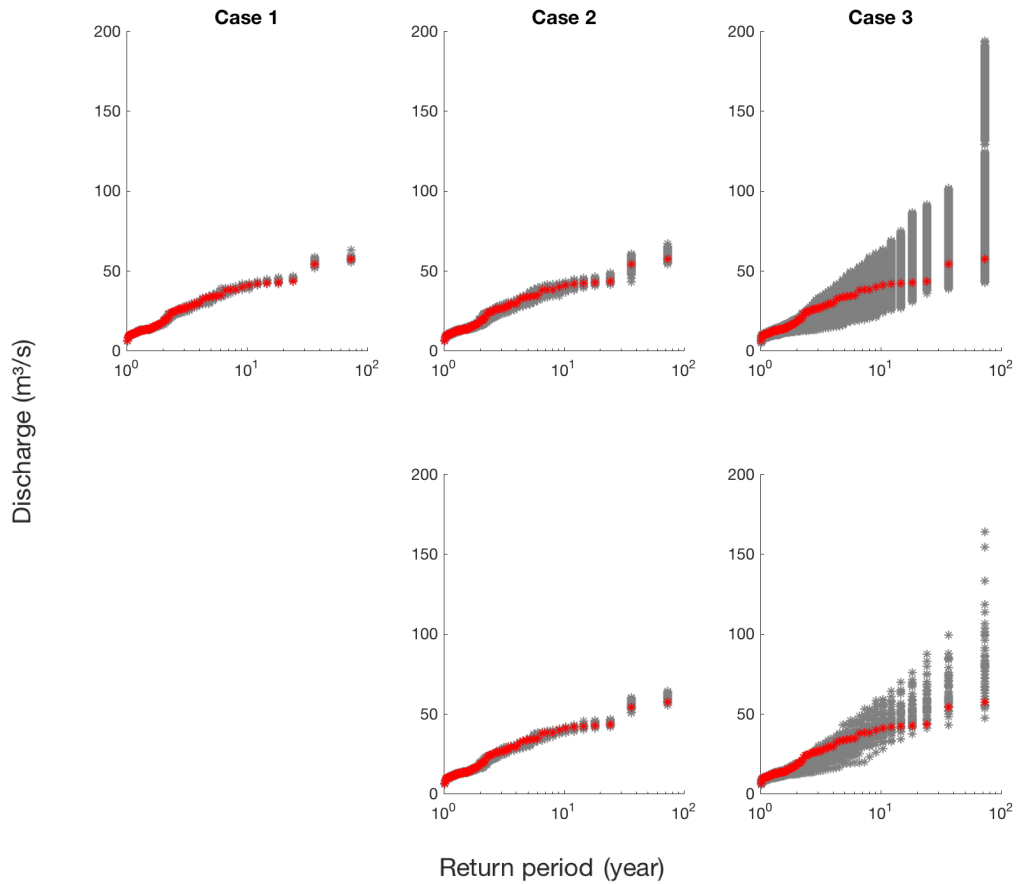


Figure 15: Comparison between the empirical return periods of annual extremes of the observed and simulated discharge for all cases: reference discharge Q_{rf} (red), the ensemble of time series of simulated discharge (grey). The top panel shows extremes obtained on the basis of unequal ensemble widths of 50 (case 1), 2500 (case 2) or 125000 (case 3) time series. The bottom panel shows extremes obtained on the basis of equal ensemble widths of 50 time series.

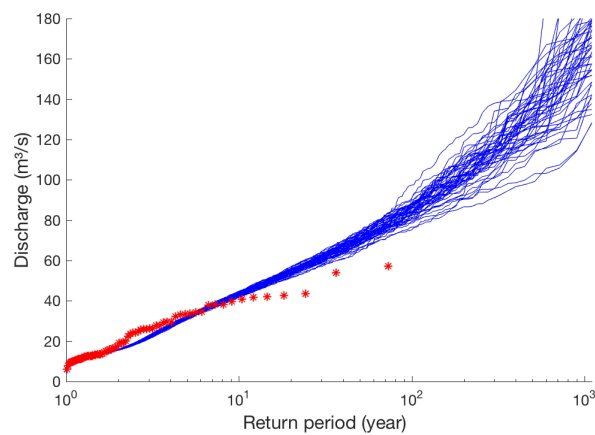


Figure 16: Comparison between the empirical return periods of annual extremes of the observed and simulated discharge for case 3 based on 50 time series of 3600 years of rainfall and corresponding evapotranspiration.

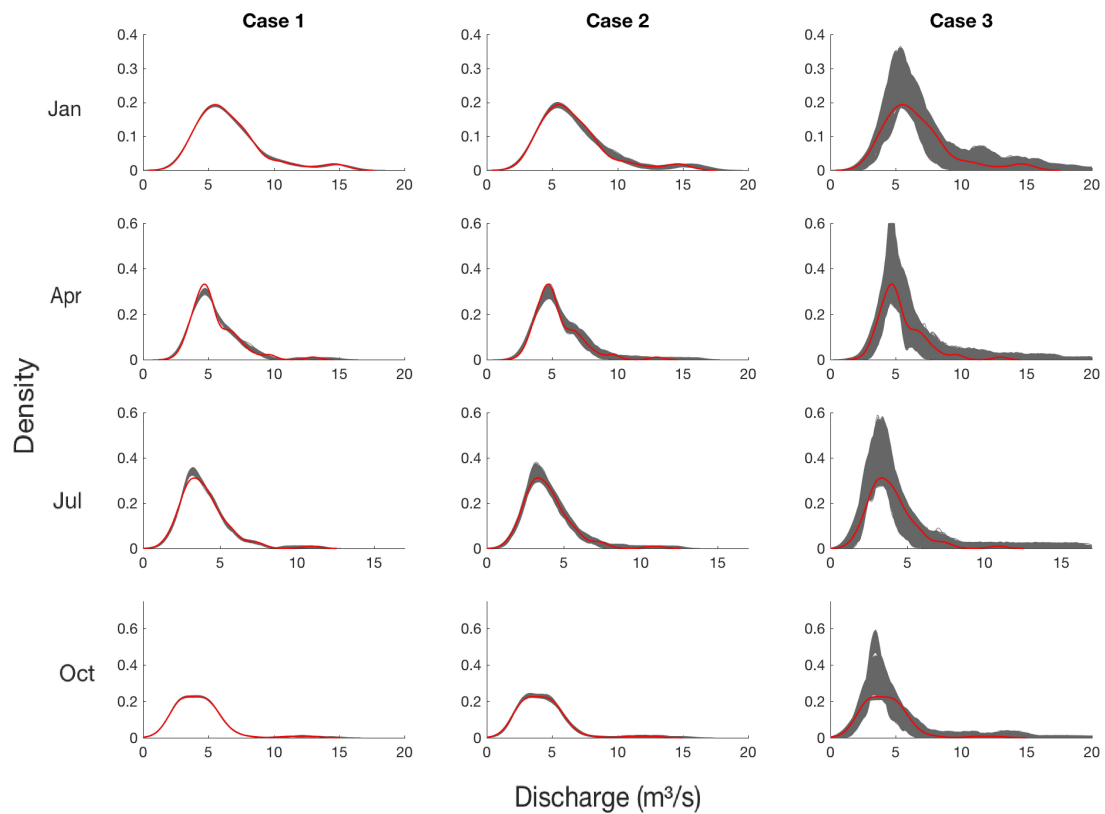


Figure 17: Comparison between the probability density functions of the mean of discharge of the observed and simulated values in three cases: reference discharge Q_{rf} (red), the time series of simulated discharge (grey).

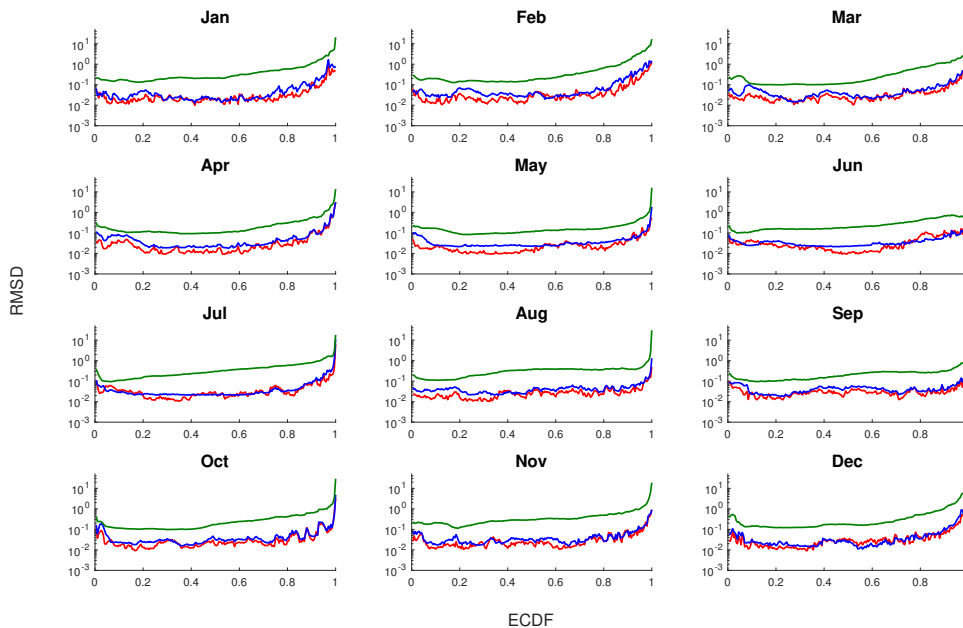


Figure 18: Root mean square difference (RMSD) for simulated discharge in different cases: case 1 (red), case 2 (blue) and case 3 (green).

494 In order to further investigate the quality of the simulated discharge for all cases, Fig. 17
 495 presents the comparison between the probability density functions of the daily averages of the
 496 modelled and reference discharge for January, April, July and October. For all cases, the daily
 497 mean seems to be preserved by the modelled discharge. However through investigating the width
 498 of the grey areas of the simulated time series for each case, as expected, we can conclude that the
 499 most certain results are observed in case 1, followed by case 2 and case 3. This also holds for the
 500 other months. Similar situations are witnessed for the univariate return period of annual extreme
 501 discharge (Fig. 15) in which the least and largest variations between the reference and simulated
 502 discharge are noticed for Q_{s1} and Q_{s3} , respectively. Especially, a remarkable expansion of grey
 503 areas is witnessed in case 3. It is clear that each stochastic component, i.e. modelled precipita-
 504 tion, temperature or evapotranspiration, has contributed an additional amount of variation to the
 505 modelled discharge. The differences between the simulated discharge from different cases are less
 506 evident in terms of probability density functions but more pronounced for the mean and extreme
 507 discharge.

508
 509 To account for the variations between the modelled and reference discharge, the simulated
 510 discharge values are further evaluated using the root mean square deviation (RMSD):

$$\text{RMSD}(i) = \sqrt{\frac{1}{n} \sum_{s=1}^n (Q_{m,s}(i) - Q_o(i))^2}, \quad (8)$$

511 where $Q_m(i)$ and $Q_o(i)$ are respectively the modelled and reference discharge value at a cumulative
 512 relative frequency $i \in [0, 1]$ and n is the number of the members in the ensemble considered.

513
 514 Figure 18 displays the RMSD calculated for simulated discharge in different cases. It can
 515 be seen from the figure that for all cases, larger RMSD values are found for the higher values of
 516 discharge. In other words, simulations of the higher values of discharge are generally less accurate.
 517 There are insignificant differences between the RMSD for case 1 and 2 for all months. The use of
 518 stochastically generated temperature time series seemed to contribute minor uncertainty to the
 519 discharge simulations in this study. The largest errors often are obtained in case 3 where the
 520 discharge is simulated from stochastically generated precipitation and evapotranspiration values.

5 Conclusions

In water management, discharge is a very important variable which can be simulated via a rainfall-runoff model using recorded precipitation and evapotranspiration data. However, in situations that suffer from data deficiency, one may consider using stochastically generated time series. In this study, the impact of using the stochastically generated precipitation and evapotranspiration on the simulation of the catchment discharge is investigated. In order to assess the influence of each stochastic variable on the discharge simulations, three different cases have been considered. In the first case, it is assumed that insufficient evapotranspiration data would be available, requiring stochastically generated evapotranspiration based on observed precipitation and temperature data by means of a copula. In the second case, where only precipitation data would be sufficiently available, the temperature and evapotranspiration are each reproduced by vine copulas. The third case addresses the situation where too short time series of observations are available. In this case, the precipitation time series could be generated using a Modified Bartlett-Lewis (MBL) model calibrated to the limited precipitation data available and then the time series of temperature and evapotranspiration could be obtained using the copula-based models. In all cases, C-vine copulas V_{TPE_pE} and V_{T_pPT} are used for the simulations of evapotranspiration and temperature, respectively. From the comparison between the simulations with the observations, the C-vine copulas seem to reproduce the time series of evapotranspiration and temperature well. It is clear that each stochastic component has a certain impact on the discharge simulations, and each additional stochastic variable will contribute an additional variation, and thus uncertainty. As expected, the simulations of the discharge obtained for case 1 show the smallest variability, while those in case 3 results in the largest variability. In general, no major differences are observed between the simulations and observations in cases 1 and 2, the characteristics of the discharge series seem to be preserved through the process for these cases. Noticeable variations are witnessed in case 3, where the discharge is simulated using modeled time series of precipitation and evapotranspiration.

With respect to extreme discharge, it was shown that the uncertainties encountered in case 3 are partly caused by the limited length of the time series used. The uncertainties on the predictions are highly reduced when input time series are used that are much longer than the maximum return period aimed at. As in this particular case, all forcing data are generated, the modeller is not restricted to the length of an observed time series, and can hence generate time series of whatever length as input to the hydrological model, taking into account that the longer the time series used, the more the uncertainty reduces at the expense of increasing run-time.

From this study, we may conclude that in situations that suffer from a lack of observations, one can rely on the stochastically generated series of precipitation, temperature and evapotranspiration to reproduce time series of discharge for water resources management. However, care should be taken as the modelled extreme discharges may experience the largest errors.

Acknowledgements

The authors gratefully acknowledge the Vietnamese Government Scholarship (VGS), the King Baudouin Foundation (KBF) and the project G.0013.11N of the Research Foundation Flanders (FWO) for their partial financial support for this work. The historical Uccle series were provided by the Royal Meteorological Institute of Belgium.

References

- Aas, K., Czado, C., Frigessi, A., and Bakken, H. (2009). Pair-copula constructions of multiple dependence. *Insurance: Mathematics and Economics*, 44(2):182–198.
- Abbott, M., Bathurst, J., Cunge, J., O’Connell, P., and Rasmussen, J. (1986). An introduction to the European Hydrological System - Système Hydrologique Européen, SHE, 1: History and

- 569 philosophy of a physically-based, distributed modelling system. *Journal of Hydrology*, 87(1):45–
570 59.
- 571 Akaike, H. (1973). Information theory and an extension of the maximum likelihood principle. In
572 *Second International Symposium on Information Theory*, Budapest. Akadémiai Kiado.
- 573 Arnold, J. G., Srinivasan, R., Muttiah, R. S., and Williams, J. R. (1998). Large area hydrologic
574 modeling and assessment. Part I: Model development. *Journal of the American Water Resources*
575 *Association (JAWRA)*, 34(1):73–89.
- 576 Bedford, T. and Cooke, R. M. (2001). *Monte Carlo Simulation of Vine Dependent Random*
577 *Variables for Applications in Uncertainty Analysis*. Management Science, theory, method and
578 practice series. University of Strathclyde, Department of Management Science.
- 579 Bedford, T. and Cooke, R. M. (2002). Vines—a new graphical model for dependent random
580 variables. *The Annals of Statistics*, 30(4):1031–1068.
- 581 Bergström, S. (1995). The HBV model. In: Singh, V.P. (Ed.) *Computer Models of Watershed*
582 *Hydrology*. Water Resources Publications, Highlands Ranch, CO., pages 443–476.
- 583 Bernardara, P., De Michele, C., and Rosso, R. (2007). A simple model of rain in time: An
584 alternating renewal process of wet and dry states with a fractional (non-Gaussian) rain intensity.
585 *Atmospheric Research*, 84(4):291–301.
- 586 Boughton, W. and Droop, O. (2003). Continuous simulation for design flood estimation - a review.
587 *Environmental Modelling and Software*, 18(4):309–318.
- 588 Cabus, P. (2008). River flow prediction through rainfall-runoff modelling with a probability –
589 distributed model (PDM) in Flanders, Belgium. *Agricultural Water Management*, 95(7):859–
590 868.
- 591 Cameron, D., Beven, K., and Tawn, J. (2000). An evaluation of three stochastic rainfall models.
592 *Journal of Hydrology*, 228(1–2):130–149.
- 593 Cowpertwait, P. S. P., Isham, V., and Onof, C. (2007). Point process models of rainfall: develop-
594 ments for fine-scale structure. *Proceedings of the Royal Society A: Mathematical, Physical and*
595 *Engineering Science*, 463(2086):2569–2587.
- 596 Czado, C. (2010). Pair-copula constructions of multivariate copulas. In Jaworski, P., Durante,
597 F., Härdle, W. K., and Rychlik, T., editors, *Copula Theory and Its Applications*, volume 198 of
598 *Lecture Notes in Statistics*, pages 93–109. Springer Berlin Heidelberg.
- 599 Dai, Y., Zeng, X., Dickinson, R. E., Baker, I., Bonan, G. B., Bosilovich, M. G., Denning, A. S.,
600 Dirmeyer, P. A., Houser, P. R., Niu, G., Oleson, K. W., Schlosser, C. A., and Yang, Z.-L. (2003).
601 The Common Land Model. *Bulletin of the American Meteorological Society*, 84(8):1013–1023.
- 602 De Jongh, I. L. M., Verhoest, N. E. C., and De Troch, F. (2006). Analysis of a 105-year time series
603 of precipitation observed at Uccle, Belgium. *International Journal of Climatology*, 26(14):2023–
604 2039.
- 605 Démarée, G. R. (2003). Le pluviographe centenaire du plateau d’ Uccle: son histoire, ses données
606 et ses applications. *Houille blanche*, 2003-004:95–102.
- 607 Droogers, P. and Allen, R. G. (2002). Estimating reference evapotranspiration under inaccurate
608 data conditions. *Irrigation and Drainage Systems*, 16(1):33–45.
- 609 Duan, Q., Sorooshian, S., and Gupta, V. K. (1994). Optimal use of the SCE-UA global optimiza-
610 tion method for calibrating watershed models. *Journal of Hydrology*, 158(3–4):265–284.
- 611 Gyasi-Agyei, Y. (1999). Identification of regional parameters of a stochastic model for rainfall
612 disaggregation. *Journal of Hydrology*, 223(34):148–163.

- 613 Heneker, T. M., Lambert, M. F., and Kuczera, G. (2001). A point rainfall model for risk-based
614 design. *Journal of Hydrology*, 247(1–2):54–71.
- 615 Joe, H. (1997). *Multivariate Models and Dependence Concepts*. Chapman & Hall, London.
- 616 Kavvas, M. L. and Delleur, J. W. (1981). A stochastic cluster model of daily rainfall sequences.
617 *Water Resources Research*, 17(4):1151–1160.
- 618 Kennedy, J. and Eberhart, R. (1995). Particle swarm optimization. In *Proceedings of the IEEE*
619 *International Conference on neural networks*, pages 1942–1948.
- 620 Khaliq, M. N. and Cunnane, C. (1996). Modelling point rainfall occurrences with the modified
621 Bartlett–Lewis rectangular pulses model. *Journal of Hydrology*, 180(1–4):109–138.
- 622 Kruskal, W. H. and Wallis, W. A. (1952). Use of ranks in one-criterion analysis of variance.
623 *Journal of the American Statistical Association*, 47:583–621.
- 624 Kurowicka, D. and Cooke, R. M. (2007). Sampling algorithms for generating joint uniform distri-
625 butions using the vine-copula method. *Computational Statistics and Data Analysis*, 51(6):2889–
626 2906.
- 627 Mason, S. J. (2004). Simulating climate over Western North America using stochastic weather
628 generators. *Climatic Change*, 62(1–3):155–187.
- 629 Moore, R. J. (2007). The PDM rainfall-runoff model. *Hydrology and Earth System Sciences*,
630 11(1):483–499.
- 631 Nelsen, R. B. (2006). *An Introduction to Copulas*. Springer, New York.
- 632 Nielsen, S. A. and Hansen, E. (1973). Numerical simulation of the rainfall-runoff process on a
633 daily basis. *Nordic Hydrol*, 3:171–190.
- 634 Ntegeka, V. and Willems, P. (2008). Trends and multidecadal oscillations in rainfall extremes,
635 based on a more than 100-year time series of 10 min rainfall intensities at Uccle, Belgium. *Water*
636 *Resources Research*, 44(7):W07402.
- 637 Onof, C., Chandler, R. E., Kakou, A., Northrop, P., Wheeler, H. S., and Isham, V. (2000). Rainfall
638 modelling using Poisson-cluster processes: a review of developments. *Stochastic Environmental*
639 *Research and Risk Assessment*, 14(6):384–411.
- 640 Onof, C. and Wheeler, H. S. (1993). Modelling of British rainfall using a random parameter
641 Bartlett–Lewis rectangular pulse model. *Journal of Hydrology*, 149(1–4):67–95.
- 642 Onof, C., Wheeler, H. S., and Isham, V. (1994). Note on the analytical expression of the inter-
643 event time characteristics for Bartlett–Lewis type rainfall models. *Journal of Hydrology*, 157(1–
644 4):197–210.
- 645 Pham, M. T., Vanhaute, W. J., Vandenberghe, S., De Baets, B., and Verhoest, N. E. C. (2013).
646 An assessment of the ability of Bartlett–Lewis type of rainfall models to reproduce drought
647 statistics. *Hydrology and Earth System Sciences*, 17(12):5167–5183.
- 648 Pham, M. T., Vernieuwe, H., De Baets, B., Willems, P., and Verhoest, N. E. C. (2016). Stochas-
649 tic simulation of precipitation-consistent daily reference evapotranspiration using vine copulas.
650 *Stochastic Environmental Research and Risk Assessment*, 30(8):2197–2214.
- 651 Rodriguez-Iturbe, I., Cox, D. R., and Isham, V. (1987a). Some models for rainfall based on
652 stochastic point processes. *Proceedings of the Royal Society of London. Series A. Mathematical*
653 *and Physical Sciences*, 410(1839):269–288.
- 654 Rodriguez-Iturbe, I., Cox, D. R., and Isham, V. (1988). A point process model for rainfall: Further
655 developments. *Proceedings of the Royal Society of London. Series A. Mathematical and Physical*
656 *Sciences*, 417(1853):283–298.

- 657 Rodriguez-Iturbe, I., De Power, B. F., and Valdes, J. B. (1987b). Rectangular pulses point process
658 models for rainfall: Analysis of empirical data. *Journal of Geophysical Research*, 92(D8):9645–
659 9656.
- 660 Salvadori, G. and De Michele, C. (2007). On the use of copulas in hydrology: Theory and practice.
661 *Journal of Hydrologic Engineering*, 12(4):369–380.
- 662 Salvadori, G., De Michele, C., Kottegoda, N., and Rosso, R. (2007). *Extremes in Nature: An*
663 *Approach Using Copulas*. Springer, New York.
- 664 Schepsmeier, U. (2015). Efficient information based goodness-of-fit tests for vine copula models
665 with fixed margins: A comprehensive review. *Journal of Multivariate Analysis*, 138:34–52.
- 666 Sklar, A. (1959). Fonctions de répartition à n dimensions et leurs marges. *Publications de l'Institut*
667 *de Statistique de l'Université de Paris*, 8:229–231.
- 668 Smithers, J. C., Pegram, G. G. S., and Schulze, R. E. (2002). Design rainfall estimation in South
669 Africa using Bartlett–Lewis rectangular pulse rainfall models. *Journal of Hydrology*, 258(14):83–
670 99.
- 671 Stern, R. D. and Coe, R. (1984). A model fitting analysis of daily rainfall data. *Journal of the*
672 *Royal Statistical Society*, 147(1):1–34.
- 673 Todorovic, P. and Woolhiser, D. A. (1975). A stochastic model of n -day precipitation. *Journal of*
674 *Applied Meteorology*, 14(1):17–24.
- 675 Vaes, G. and Berlamont, J. (2000). Selection of appropriate short rainfall series for design of
676 combined sewer systems. In *Proceedings of 90 International Conference on Urban Drainage on*
677 *Internet, Hydroinform, Czech Republic*.
- 678 Vandenberghe, S., Verhoest, N. E. C., Buyse, E., and De Baets, B. (2010). A stochastic design
679 rainfall generator based on copulas and mass curves. *Hydrology and Earth System Sciences*,
680 14(12):2429–2442.
- 681 Vanhaute, W., Vandenberghe, S., Scheerlinck, K., De Baets, B., and Verhoest, N. E. C. (2012).
682 Calibration of the modified Bartlett–Lewis model using global optimization techniques and
683 alternative objective functions. *Hydrology and Earth System Sciences*, 16(3):873–891.
- 684 Velghe, T., Troch, P. A., De Troch, F. P., and Van de Velde, J. (1994). Evaluation of cluster-based
685 rectangular pulses point process models for rainfall. *Water Resources Research*, 30(10):2847–
686 2857.
- 687 Verhoest, N. E. C., Troch, P., and De Troch, F. (1997). On the applicability of Bartlett–Lewis
688 rectangular pulses models in the modeling of design storms at a point. *Journal of Hydrology*,
689 202(14):108–120.
- 690 Verhoest, N. E. C., Vandenberghe, S., Cabus, P., Onof, C., Meca-Figueras, T., and Jameled-
691 dine, S. (2010). Are stochastic point rainfall models able to preserve extreme flood statistics?
692 *Hydrological Processes*, 24(23):3439–3445.
- 693 Viglione, A., Castellarin, A., Rogger, M., Merz, R., and Blöschl, G. (2012). Extreme rainstorms:
694 Comparing regional envelope curves to stochastically generated events. *Water Resources Re-*
695 *search*, 48(1):W01509.
- 696 Vrebos, D., Vansteenkiste, T., Staes, J., Willems, P., and Meire, P. (2014). Water displacement by
697 sewer infrastructure in the Grote Nete catchment, Belgium, and its hydrological regime effects.
698 *Hydrology and Earth System Sciences*, 18(3):1119–1136.
- 699 Welch, B. (1951). On the comparison of several mean values: an alternative approach. *Biometrika*,
700 38(3–4):330–336.

- 701 Wilks, D. S. (1998). Multisite generalization of a daily stochastic precipitation generation model.
702 *Journal of Hydrology*, 210(1–4):178–191.
- 703 Wilks, D. S. and Wilby, R. L. (1999). The weather generation game: a review of stochastic weather
704 models. *Progress in Physical Geography*, 23(3):329–357.
- 705 Willems, P. (2013). Adjustment of extreme rainfall statistics accounting for multidecadal climate
706 oscillations. *Journal of Hydrology*, 490:126–133.
- 707 Woolhiser, D. A. and Roldán, J. (1982). Stochastic daily precipitation models: 2. A comparison
708 of distributions of amounts. *Water Resources Research*, 18(5):1461–1468.